SI Appendix for "Ambiguity in the causes for decadal trends in atmospheric methane and hydroxyl"

Alexander J. Turner, Christian Frankenberg, Paul O. Wennberg, & Daniel J. Jacob

December 23, 2016

Contents

1 A criticism of the isotope analysis in Schaefer *et al.* (2016)

1.1 Abstract

Schaefer *et al.*[1] conclude that fossil-fuel methane sources did not cause the renewed growth in atmospheric methane because its isotopic signature ($\delta^{13}CH_4$) is too heavy. However, fossil-fuel sources are not strictly thermogenic in origin and past work has measured fossil-fuel sources with $\delta^{13}CH_4$ that could explain 0% to 100% of the renewed growth in atmospheric methane since 2007.

1.2 Comment

To understand the reasons for changes in atmospheric methane since the 1990s, Schaefer *et al.*[1] examined global trends in atmospheric methane and measurements of bulk carbon isotope ratios in atmospheric methane ($\delta^{13}CH_4$) from 17 sites. They use these 17 records to construct a globally averaged isotope ratio in atmospheric methane ($\delta^{13}CH_{4(atm)}$). Their data set shows a 0.5‰ increase in $\delta^{13}CH_{4(atm)}$ from 1980 to 1998, a constant $\delta^{13}CH_{4(atm)}$ of -47.2‰ from 1998 to 2008, and a 0.2‰ decrease in $\delta^{13}CH_{4(atm)}$ from 2008 to 2014. Schaefer *et al.*[1] posit that different sources and sinks have distinct isotopic signatures that can be used to determine the sources causing these changes in $\delta^{13}CH_{4(atm)}$. Specifically, Schaefer *et al.*[1] assume that pyrogenic, thermogenic, and biogenic methane sources have isotopic signatures of -22‰, -37‰, and -60‰, respectively.

Schaefer *et al.*[1] then create reconstructions of atmospheric methane concentrations and $\delta^{13}CH_{4(atm)}$ using emission perturbations from sources with different isotopic signatures. They find that a +19.7 Tg a^{-1} source with an average isotopic signature ($\delta^{13}CH_{4(so)}$) of -59‰ best explains the observed decrease in $\delta^{13}CH_{4(atm)}$ from 2008 to 2014. Based on this, they conclude that biogenic methane sources are responsible for the renewed growth because $\delta^{13}CH_{4(so)}$ matches their assumed isotopic signature for biogenic methane sources. A major conclusion from the abstract of Schaefer *et al.*[1] is: "*Thermogenic emissions didn't resume to cause the renewed [CH_4]-rise after 2006*" and from their conclusions: "*Importantly, they [fossil-fuel emissions] are a minor contributor to the renewed [CH_4]-rise.*"

Schaefer *et al.*[1] reach the latter conclusion because they assume that fossil-fuel sources emit thermogenic methane. However, fossil-fuel sources are not strictly thermogenic in origin. In fact, over 20% of the world's natural gas accumulations are of biogenic origin[2]. Biogenic gas is particularly common in non-conventional gas resources such as coalbed methane and organic shale gas basins[3]. Numerous US basins with non-conventional natural gas resources have been found to be predominately biogenic methane (e.g., the Antrim Shale[3, 4, 5], the New Albany Shale[4], and the Powder River Basin[6]).

As such, fossil-fuel and non-fossil methane sources have overlapping isotopic signatures. Table S1 lists measured methane isotope compositions for various sources compiled from previous work[7, 8, 6, 5, 9]. From Table S1, we find fossil-fuel methane isotope signatures ($\delta^{13}CH_{4(ff)}$) that range from -15‰ to -76‰ and non-fossil methane isotope signatures ($\delta^{13}CH_{4(nf)}$) that range from -31‰ to -93‰. Recently, Stolper *et al.*[5] found a $\delta^{13}CH_{4(ff)}$ of -58.0‰ to -60.4‰ for methane samples collected from boreholes in the Gulf of Mexico and Wang *et al.*[6] found a $\delta^{13}CH_{4(ff)}$ of -58.6‰ to -62.0‰ for methane sampled from multiple gas wells in the Powder River Basin. Both of these fossil-fuel methane sources have a $\delta^{13}CH_4$ that match the best-fit $\delta^{13}CH_{4(so)}$ from Schaefer *et al.*[1].

Table 1: Measured methane isotope compositions ($\delta^{13}CH_4$) for various sources.

Source[a]	$\delta^{13}CH_4$	Gas Type[b]	Reference
fossil-fuel (-15‰ to -76‰)			
Powder River Basin	-58.6‰ to -62.0‰	B	Wang *et al.*[6][c]
Gulf of Mexico	-58.0‰ to -60.4‰	B	Stolper *et al.*[5][d]
Antrim Shale	-50.2‰ to -53.2‰	M	Stolper *et al.*[5][d], Stolper *et al.*[10][e]
Potiguar Basin	-37.4‰ to -49.6‰	T	Stolper *et al.*[5][d]
Guyamas Basin	-44.0‰	T	Wang *et al.*[6][c]
Haynesville Shale	-35.2‰ to -38.9‰	T	Stolper *et al.*[5][d]
Marcellus Shale	-34.2‰ to -35.8‰	T	Stolper *et al.*[5][d]
North Appalachia Basin	-25.7‰ to -36.2‰	T	Wang *et al.*[6][c]
Coal-associated gas	-15‰ to -70‰	M	Bréas *et al.*[7][f]
Oil-associated gas	-30‰ to -60‰	M	Bréas *et al.*[7][f]
Gas drilling, pipeline leakage	-41‰ to -76‰	M	Bréas *et al.*[7][f]
Biomass Burning (C4 vegetation)	-17 ± 3‰	P	Dlugokencky *et al.*[8][g]
Biomass Burning (C3 vegetation)	-26 ± 3‰	P	Dlugokencky *et al.*[8][g]
Biomass Burning	-24‰ to -32‰	P	Bréas *et al.*[7][f]
non-fossil (-31‰ to -93‰)			
Hydrates (North Cascadia Margin)	-61.6‰ to -68.5‰	B	Wang *et al.*[6][c]
Pennsylvania Dairy Cows (C4 diet)	-52.8‰ to -54.2‰	B	Wang *et al.*[6][c]
Ruminants (C3 diet)	-61‰ to -76‰	B	Bréas *et al.*[7][f]
Ruminants (C4 diet)	-47‰ to -55‰	B	Bréas *et al.*[7][f]
Swamp (Massachusetts)	-59.2‰ to -59.7‰	B	Wang *et al.*[6][c]
Swamp (California)	-63.8‰ to -68.0‰	B	Wang *et al.*[6][c]
Lake (Massachusetts)	-65.5‰ to -71.0‰	B	Wang *et al.*[6][c]
Wetlands (Bogs)	-51‰ to -85‰	B	Bréas *et al.*[7][f]
Wetlands (Swamps)	-31‰ to -73‰	B	Bréas *et al.*[7][f]
Rice Paddies	-50‰ to -68‰	B	Bréas *et al.*[7][f]
Landfills	-52‰ to -63‰	B	Bréas *et al.*[7][f]
Termites	-44‰ to -93‰	B	Bréas *et al.*[7][f]
Isotope signatures assumed in Schaefer et al.[1]			
Pyrogenic	-22‰	P	Dlugokencky *et al.*[8], Bréas *et al.*[7]
Thermogenic	-37‰	T	Dlugokencky *et al.*[8], Bréas *et al.*[7]
Biogenic	-60‰	B	Dlugokencky *et al.*[8], Bréas *et al.*[7]

[a] We have included biomass burning in the "fossil-fuel" category, as Bréas *et al.*[7] did.
[b] "P" is pyrogenic, "T" is thermogenic, "B" is biogenic, and "M" is mixed biogenic and thermogenic.
[c] Table S1 in Wang *et al.*[6].
[d] Table S2 in Stolper *et al.*[5].
[e] Table 3 in Stolper *et al.*[10].
[f] Table 4 in Bréas *et al.*[7].
[g] Table 1 in Dlugokencky *et al.*[8].

We can use the isotope mass-balance to compute the fraction of emissions from fossil-fuel methane sources (f):

$$f = \frac{E_{(\mathrm{ff})}}{E_{(\mathrm{so})}} = \frac{\delta^{13}\mathrm{CH}_{4(\mathrm{so})} - \delta^{13}\mathrm{CH}_{4(\mathrm{nf})}}{\delta^{13}\mathrm{CH}_{4(\mathrm{ff})} - \delta^{13}\mathrm{CH}_{4(\mathrm{nf})}} \quad (1)$$

where $E_{(\mathrm{ff})}$ is the potential increase in fossil-fuel methane emissions and $E_{(\mathrm{so})}$ is the increased emissions required to explain the renewed increase in atmospheric methane, Schaefer *et al.*[1] find $E_{(\mathrm{so})} = +19.7$ Tg a^{-1}.

Fig. S1 shows the fraction of the renewed growth in atmospheric methane attributable to fossil-fuel sources over the plausible range of fossil-fuel and non-fossil methane isotope signatures from Table S1. Fig. 1 uses the best-fit $\delta^{13}\mathrm{CH}_{4(\mathrm{so})}$ of -59‰ from Schaefer *et al.*[1]. Not surprisingly, we find that a fossil-fuel or non-fossil methane source with a $\delta^{13}\mathrm{CH}_4$ of -59‰ could explain 100% of the observed changes in $\delta^{13}\mathrm{CH}_{4(\mathrm{atm})}$. However, there are also other plausible scenarios where fossil-fuel methane sources could explain between 0% and 100% of the observed changes in $\delta^{13}\mathrm{CH}_{4(\mathrm{atm})}$. For example, an increase in methane emissions that is 55% fossil-fuel and 45% non-fossil with isotope signatures of -50‰ and -70‰, respectively, could also explain the observed changes in $\delta^{13}\mathrm{CH}_{4(\mathrm{atm})}$.

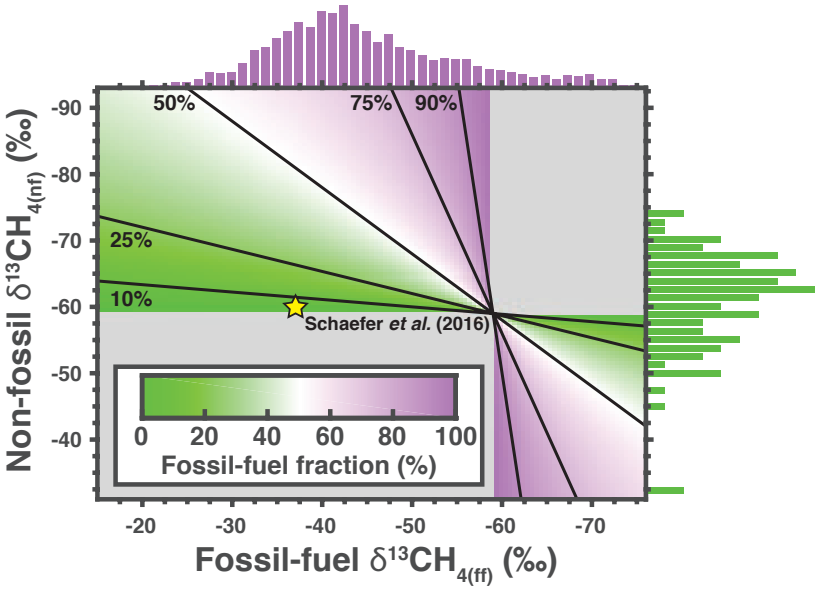

Figure 1: Fraction of renewed growth since 2007 in atmospheric methane attributable to fossil-fuel methane sources (f). Computed using Eq. 1 with a $\delta^{13}\mathrm{CH}_{4(\mathrm{so})}$ of -59‰, the best fit $\delta^{13}\mathrm{CH}_{4(\mathrm{so})}$ from Schaefer *et al.*[1]. The x- and y-axes span the range of $\delta^{13}\mathrm{CH}_4$ measured for fossil-fuel and non-fossil methane sources from Table S1. Pink (green) histogram is the distribution of fossil-fuel (non-fossil) isotopic signatures from Schwietzke *et al.*[11]. Gray areas indicate non-physical solutions. Yellow star is the assumed isotopic signatures from Schaefer *et al.*[1]: $\delta^{13}\mathrm{CH}_{4(\mathrm{nf})} = -60$‰ and $\delta^{13}\mathrm{CH}_{4(\mathrm{ff})} = -37$‰.

In contrast to Schaefer *et al.*[1], our analysis presented here demonstrates that an increase in fossil-fuel methane sources could be a major contributor to the renewed growth in atmospheric methane since 2007. Given the overlapping isotope signatures of fossil-fuel and non-fossil sources, future work should be cautious when interpreting changes in $\delta^{13}\mathrm{CH}_{4(\mathrm{atm})}$.

2 Additional information on the observations, hemispheric averages, and model

We use publicly available data from NOAA/ESRL, INSTAAR, U.C. Irvine, U. Washington, GAGE, and AGAGE. For methane observations, we use 92 monitoring stations from the NOAA/ESRL global monitoring network. For $\delta^{13}CH_4$ we use 32 monitoring sites from NOAA/ESRL/INSTAAR, U.C. Irvine, and U. Washington (see Table S2). For methyl chloroform we use 22 sites from NOAA/ESRL, GAGE, and AGAGE (see Table S2).

Fig. S2 shows the individual de-seasonalized observational records and the bootstrapped hemispheric averages with uncertainties. The process for obtaining the hemispheric averages and uncertainties is as follows:

1. De-seasonalize each observational record with a stable seasonal filter and a 1-year moving average.
2. Group each de-seasonalized observational record by hemisphere and determine the number of sites in the Northern (Southern) hemisphere: n_N (n_S).
3. Randomly select n_N (n_S) records from the Northern (Southern) hemisphere with replacement.
4. Compute the hemispheric average from the randomly selected n_N (n_S) records.
5. Repeat n_B times, yielding n_B different hemispheric averages.
6. Compute the mean hemispheric average and standard deviation from the n_B realizations.

We use a reaction rate for OH + CH_4 of 3.4×10^{-15} cm^3 $molec^{-1}$ s^{-1} (derived from the three-parameter expression: $k(T) = 2.80 \times 10^{-14} T^{0.667} \exp(-1575/T)$ from Burkholder *et al.*[12] using a temperature of 270 K) and a kinetic isotope effect (KIE) of 1.005 from Burkholder *et al.*[12] (originally from Cantrell *et al.*[13]: 1.005±0.002). Our simple 2-box model neglects minor methane sinks (methanotrophic bacteria in aerated soils, chlorine and atomic oxygen radicals in the stratosphere, and chlorine radicals from sea salt in the marine boundary layer) and only considers a single loss process for atmospheric methane: reaction with OH. As such, we could be aliasing errors from those minor loss pathways onto the estimated OH concentrations.

3 Other output from the main text inversions

This section presents additional output from the main text inversions. Specifically, we present the inter-hemispheric difference, the methyl chloroform emissions, and the residuals.

Fig. S3 shows the inter-hemispheric differences (IHD) of atmospheric methane and $\delta^{13}CH_4$ as well as the underlying drivers for the simulated IHD. We find that the posterior simulation is able to capture most of the IHD in in atmospheric methane and $\delta^{13}CH_4$. The most prominent feature in the IHD is the minimum from 1989 to 1993. In our posterior simulation, this minimum is due to a slight (∼7 Tg/yr) increase in Southern hemispheric methane emissions.

Fig. S4 shows the methyl chloroform emissions from the the main text inversions as well as the emissions from Prinn *et al.*[14], used as a prior. All three inversions find that the Prinn *et al.*[14] emissions are, generally, overestimated before 2000.

Table 2: Monitoring stations used for $\delta^{13}CH_4$ and methyl chloroform.

Station	Code	Latitude	Laboratory
isotope measurements			
Alert, Canada	ALT	82°N	NOAA/ESRL/INSTAAR
Ascension Island, UK	ASC	8°S	NOAA/ESRL/INSTAAR
Terceira Island, Azores	AZR	39°N	NOAA/ESRL/INSTAAR
Baring Head, NZ	BHD	41°S	NOAA/ESRL/INSTAAR
Barrow, USA	BRW	71°N	NOAA/ESRL/INSTAAR
Cold Bay, USA	CBA	55°N	NOAA/ESRL/INSTAAR
Cape Grim, Australia	CGO	41°S	NOAA/ESRL/INSTAAR
Cape Kumukahi, USA	KUM	20°N	NOAA/ESRL/INSTAAR
Lac La Biche, Canada	LLB	55°N	NOAA/ESRL/INSTAAR
High Altitude Global Climate Observation Center, Mexico	MEX	19°N	NOAA/ESRL/INSTAAR
Mace Head, Ireland	MHD	53°N	NOAA/ESRL/INSTAAR
Mauna Loa, USA	MLO	20°N	NOAA/ESRL/INSTAAR
Niwot Ridge, USA	NWR	40°N	NOAA/ESRL/INSTAAR
Cape Matatula, Samoa	SMO	14°S	NOAA/ESRL/INSTAAR
South Pole, Antarctica	SPO	90°S	NOAA/ESRL/INSTAAR
Summit, Greenland	SUM	73°N	NOAA/ESRL/INSTAAR
Tae-ahn Peninsula, Korea	TAP	37°N	NOAA/ESRL/INSTAAR
Mt. Waliguan, China	WLG	36°N	NOAA/ESRL/INSTAAR
Ny-Alesund, Norway	ZEP	80°N	NOAA/ESRL/INSTAAR
Alert, Canada	ALT	82°N	U. Heidelberg
Izana, Portugal	IZA	28°N	U. Heidelberg
Neumayer, Antarctica	NEU	71°S	U. Heidelberg
Niwot Ridge, USA	NWR	41°N	U.C. Irvine
Montana de Oro, USA	MDO	35°N	U.C. Irvine
Cape Grim, Australia	CGO	41°S	U. Washington
Olympic Peninsula, USA	OPW	48°N	U. Washington
Fraserdale, Canada	FSD	50°N	U. Washington
Majuro, Marshall Islands	MMI	7°N	U. Washington
Mauna Loa, USA	MLO	19°N	U. Washington
Baring Head, NZ	BHD	41°S	U. Washington
Barrow, USA	BRW	71°N	U. Washington
Tutuila, Samoa	SMO	14°S	U. Washington
methyl chloroform measurements			
Alert, Canada	ALT	82°N	NOAA/ESRL
Barrow, USA	BRW	71°N	NOAA/ESRL
Cape Grim, Australia	CGO	41°S	NOAA/ESRL
Cape Kumukahi, USA	KUM	20°N	NOAA/ESRL
Mace Head, Ireland	MHD	53°N	NOAA/ESRL
Mauna Loa, USA	MLO	20°N	NOAA/ESRL
Palmer Station, Antarctica	PSA	65°S	NOAA/ESRL
Niwot Ridge, USA	NWR	40°N	NOAA/ESRL
Cape Matatula, Samoa	SMO	14°S	NOAA/ESRL
South Pole, Antarctica	SPO	90°S	NOAA/ESRL
Summit, Greenland	SUM	73°N	NOAA/ESRL
Trinidad Head, USA	THD	41°N	NOAA/ESRL
Cape Grim, Australia	CGO	41°S	GAGE
Mace Head, Ireland	MHD	53°N	GAGE
Cape Meares, USA	ORG	45°N	GAGE
Ragged Point Barbados	RPB	13°N	GAGE
Cape Matatula, Samoa	SMO	14°S	GAGE
Cape Grim, Australia	CGO	41°S	AGAGE
Mace Head, Ireland	MHD	53°N	AGAGE
Ragged Point Barbados	RPB	13°N	AGAGE
Cape Matatula, Samoa	SMO	14°S	AGAGE
Trinidad Head, USA	THD	41°N	AGAGE

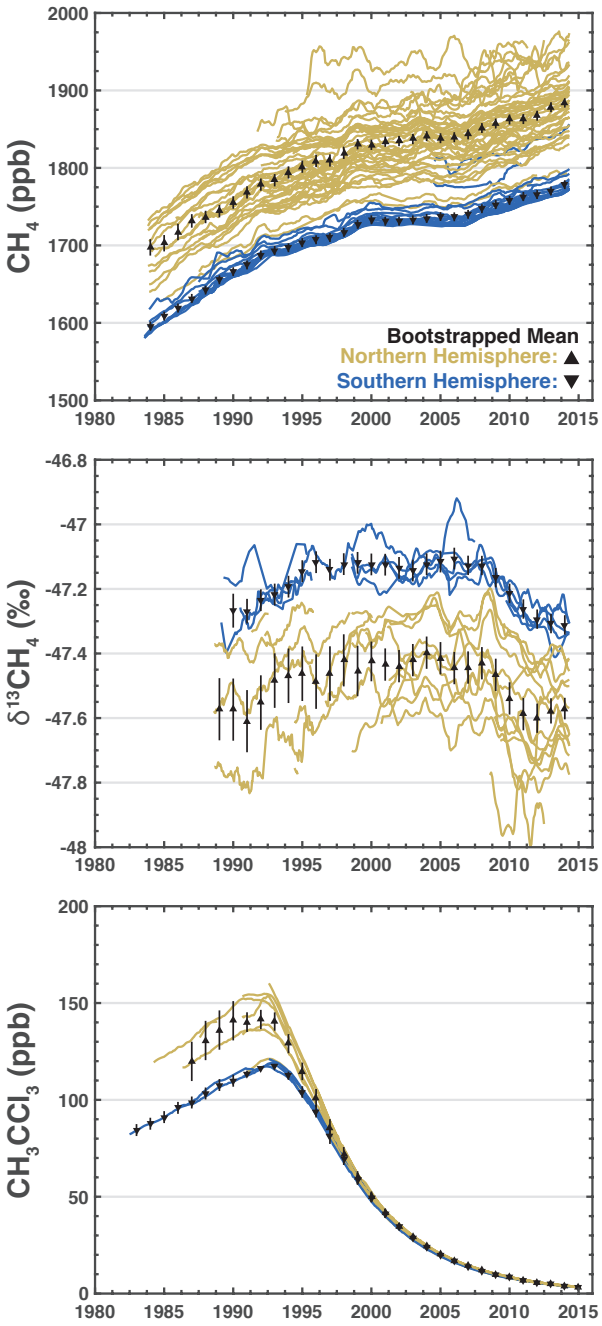

Figure 2: Bootstrapped hemispheric averages and uncertainties. Each line is the de-seasonalized time-series from a single site colored by hemisphere (Northern hemisphere is yellow and Southern hemisphere is blue). The black triangles are the annual hemispheric means and the error bars are the uncertainty derived from the bootstrapping. Top panel is the methane observations, middle panel is the $\delta^{13}CH_4$ observations, and the bottom panel is the methyl chloroform observations.

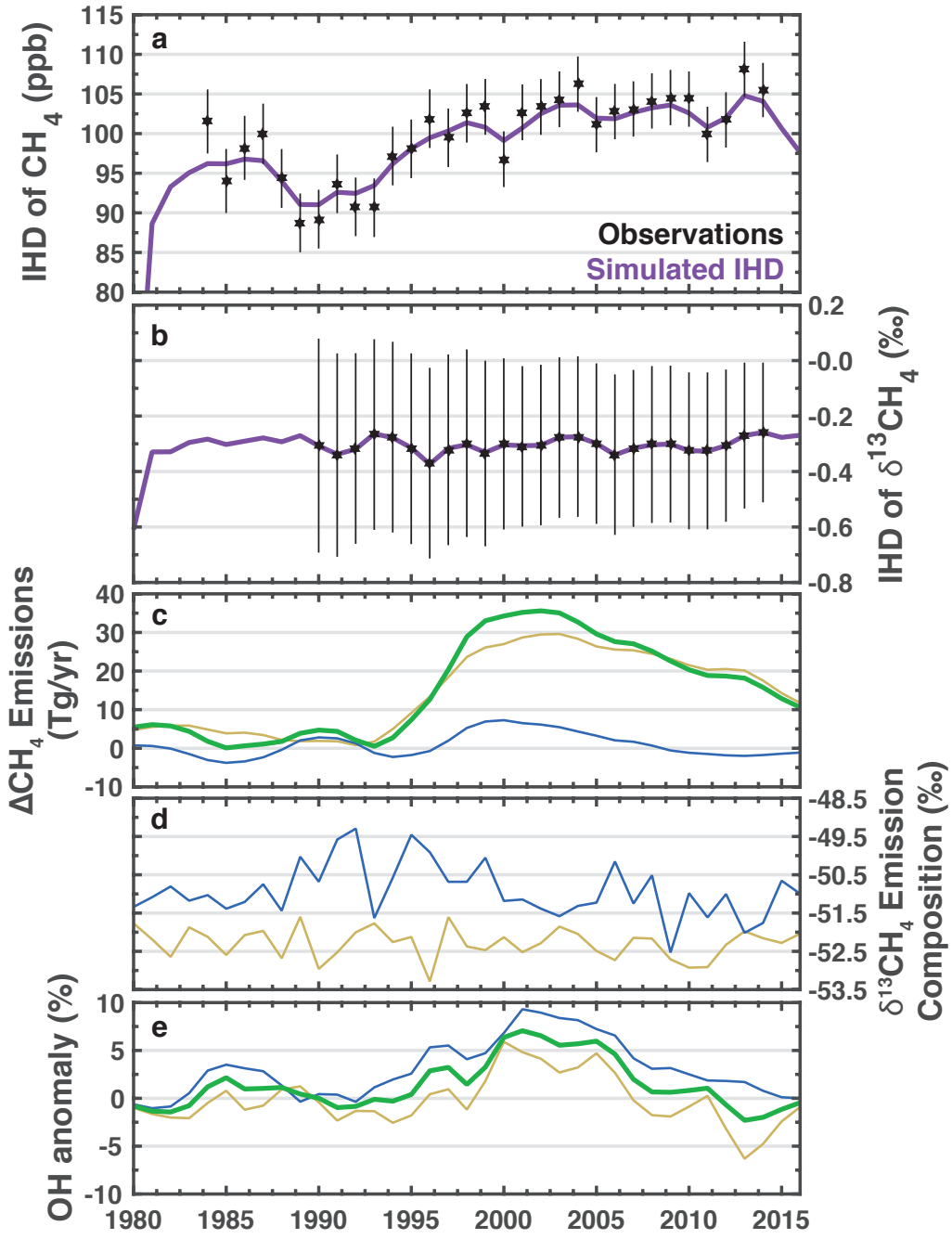

Figure 3: Inter-hemispheric difference (IHD) of atmospheric methane and $\delta^{13}CH_4$. (**a**) Inter-hemispheric difference of atmospheric methane. Black stars are the observed IHD and solid purple line is the simulated IHD using the most likely solution from the non-linear inversion. (**b**) Inter-hemispheric difference of $\delta^{13}CH_4$ in atmospheric methane. (**c**–**e**) Same as right column from main text Fig. 2. Drivers of the decadal trends in atmospheric methane. Green line is the global value, yellow line is the Northern hemisphere, and blue line is the Southern hemisphere.

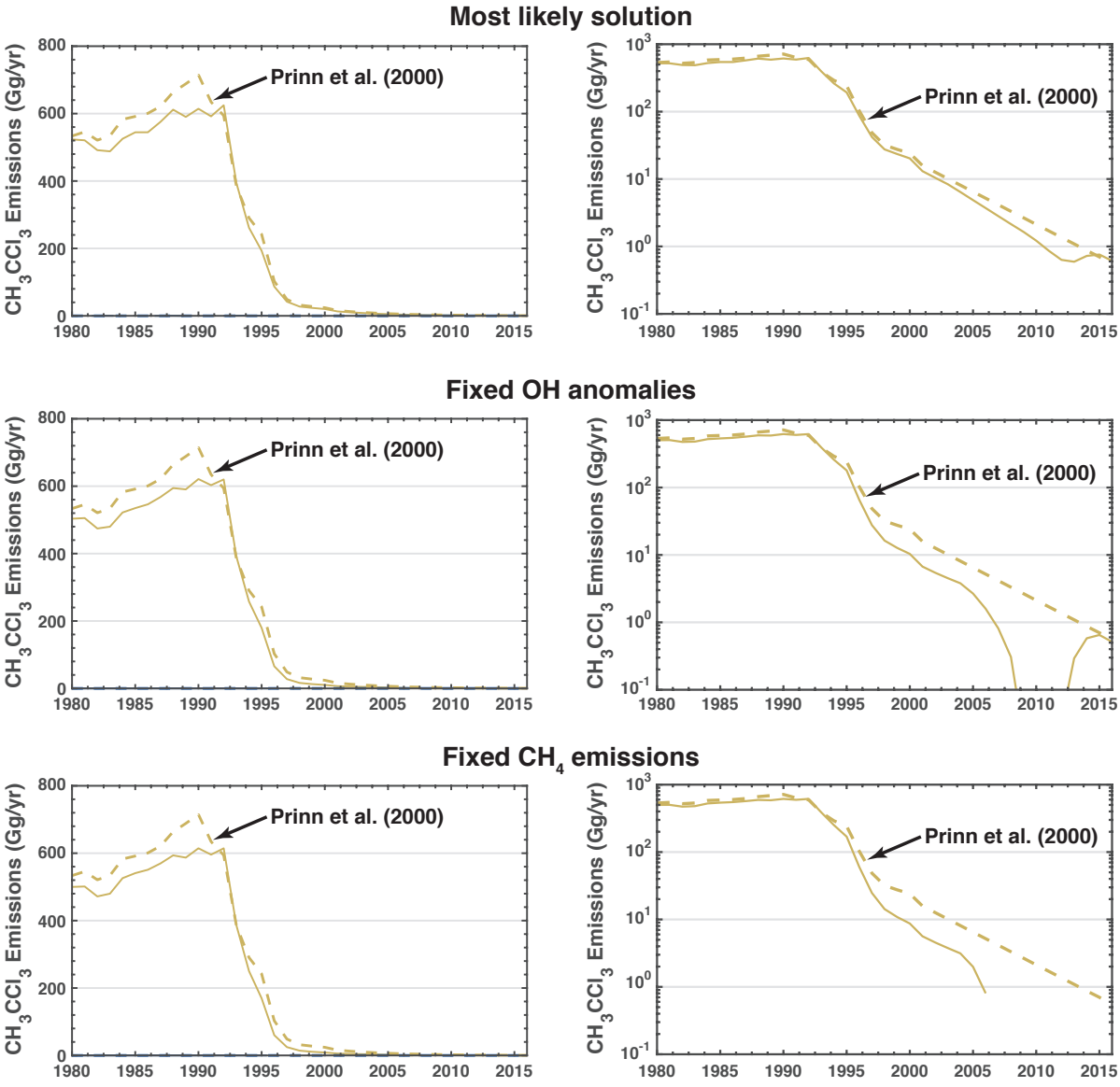

Figure 4: Methyl chloroform emissions. Top row shows the emissions from the most likely solution, middle row shows the fixed OH case, and bottom row shows the fixed methane emissions case. Left column is a linear scale and right column is a log scale. Dashed line in all panels is the Prinn *et al.*[14] emissions used as a prior for the inversions. Note that the posterior solution does allow for negative emissions (uptake by the oceans) and are not shown in the log-scale column.

Figs. S5, S6, and S7 show the residuals from the most likely solution, the fixed OH case, and the fixed methane emissions case, respectively. We can see that in all cases the uncertainty in the residuals bounds zero. However, we do find a systematic overestimate in the methyl chloroform observations before 2000. This overestimate is due to three factors: (1) using a Gaussian (or Gaussian-like) prior in the inversions, the (2) the methyl chloroform are overestimated before 2000, and (3) the large uncertainty in the early methyl chloroform observations. These three factors lead to a systematic overestimate in the methyl chloroform observations prior to 2000. Although as mentioned before, the uncertainty in the overestimate bounds zero.

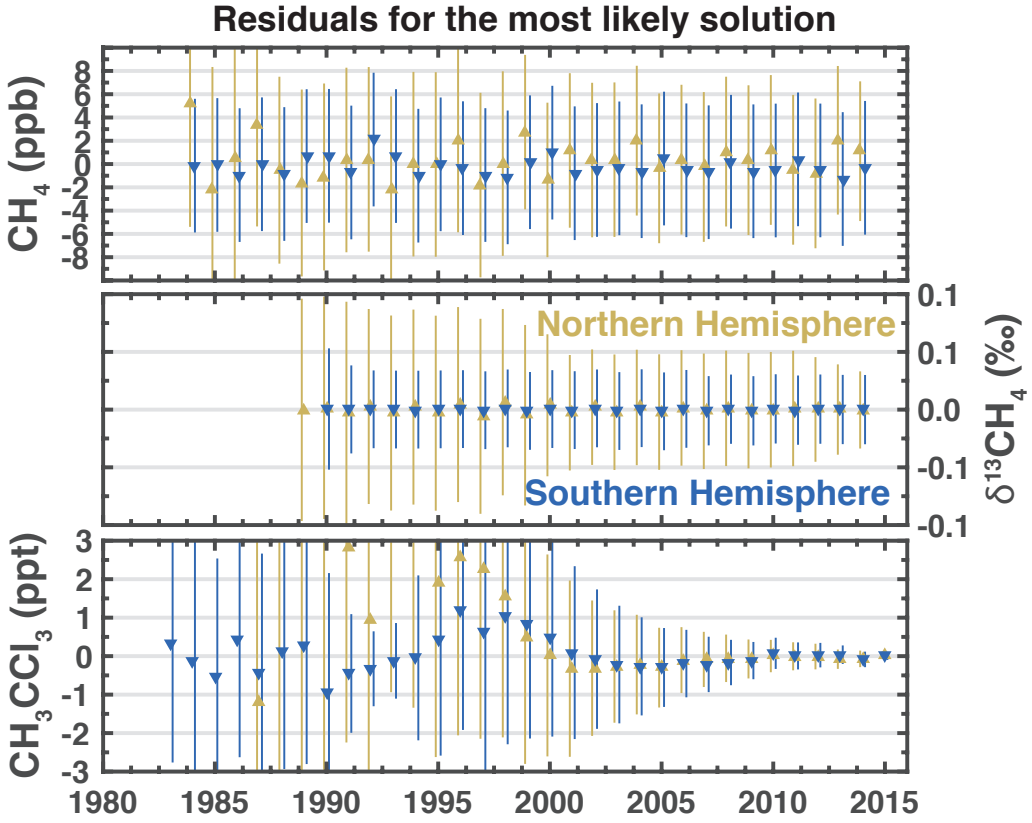

Figure 5: Residuals for the most likely solution. Top panel shows the residuals for the methane observations, middle planel is the $\delta^{13}CH_4$ observations, and bottom panel is the methyl chloroform observations. Yellow is the Northern hemisphere and blue is the southern hemisphere.

4 Additional sensitivity tests

This section presents additional sensitivity tests. All the additional sensitivity tests were done using a simple linear Gaussian inversion. Overall, we find that the magnitude of the drivers is sensitive to the assumed uncertainty but the temporal patterns are, reasonably, robust.

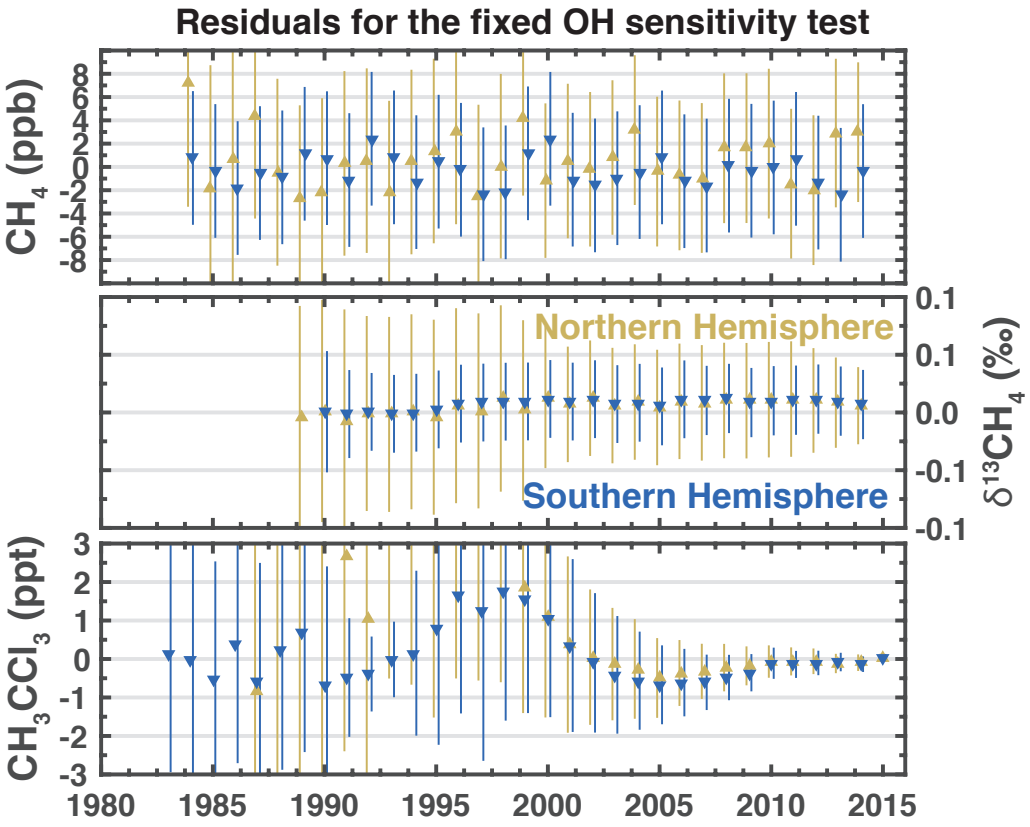

Figure 6: Same as Fig. S6 but for the sensitivity test with fixed OH (main text Fig. 4).

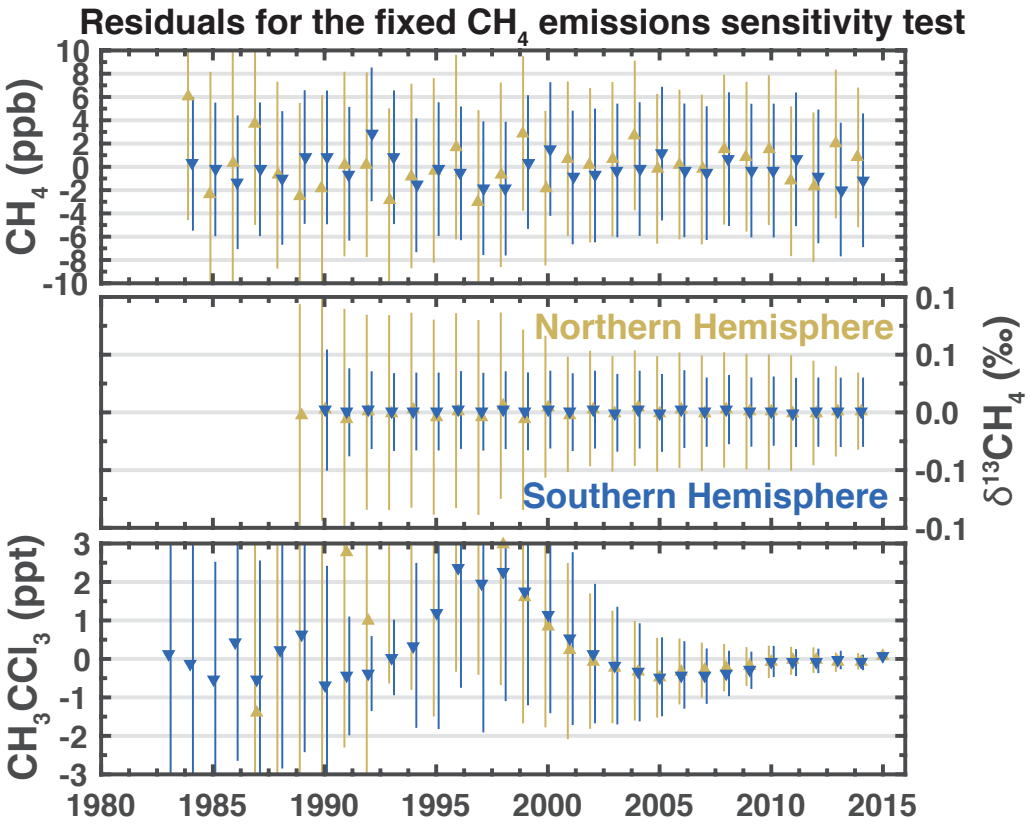

Figure 7: Same as Fig. S7 but for the sensitivity test with fixed methane emissions (main text Fig. 5).

4.1 Varying the prior uncertainties

We performed additional inversions where the uncertainty in the methane emissions was varied (Fig. S8) and the uncertainty in the OH anomalies was varied (Fig. S9). Overall, we find that the magnitude of the drivers is sensitive to the assumed uncertainty but the temporal patterns are (reasonably) robust.

4.2 Alternate hemispheric averages

We tested the sensitivity to the hemispheric averaging scheme by using an alternate set of hemispheric averages. The CH_4 and $\delta^{13}CH_4$ averages were provided by E. Dlugokencky (E. Dlugokencky, NOAA/ESRL, personal communication; data included in tarball with code) and the methyl chloroform averages were from NOAA/ESRL (see the "`combined/HATS_global_MC.txt`" file). The alternate hemispheric averages for CH_4 and $\delta^{13}CH_4$ did not report an uncertainty, so we assume the same uncertainty as the bootstrapping method presented in Section 2. Fig. S10 shows the resulting hemispheric averages from the two schemes.

The overall spatial and temporal patterns for the methane emissions and OH anomalies are largely unaffected (see Fig. S11). The only major difference is in the resulting $\delta^{13}CH_4$ emission composition

4.3 Varying the methyl chloroform parameters

The methyl chloroform residuals have a potential systematic difference between 1995 and 2000 (see Figs. S5, 6, and 7). In all cases the uncertainty on the residuals bound zero. Additionally, our most likely solution has the smallest residual during this period. Nevertheless, we investigate the potential impact of this systematic residual.

We performed two sensitivity tests to look at the impact of the residual:

1. Limit the uncertainty in methyl chloroform observations to 2 ppt.
2. Smooth the methyl chloroform emissions from Prinn *et al.*[14] with a 5-year filter.
3. Limit the uncertainty and smooth the methyl chloroform emissions.

Fig. S12 shows the original methyl chloroform emissions and the smoothed emissions. Fig. S13 shows the main drivers from three cases we investigated as well as the residuals. The conclusions from the work are, largely, unaffected by the treatment of methyl chloroform emissions in the early part of the record.

Case #1 and #3 result in larger changes in OH and methane emissions in the late 1980s and early 1990s. This is because the uncertainty in the observations is reduced, resulting in the observations carrying more weight. Case #2 does not result in qualitatively different drivers (Fig. S12).

4.4 Varying the interhemispheric exchange time

We performed additional inversions where we varied the interhemispheric exchange time (τ). Fig. S14. Overall, we find that the magnitude of the drivers is sensitive to the assumed uncertainty but the temporal patterns are (reasonably) robust.

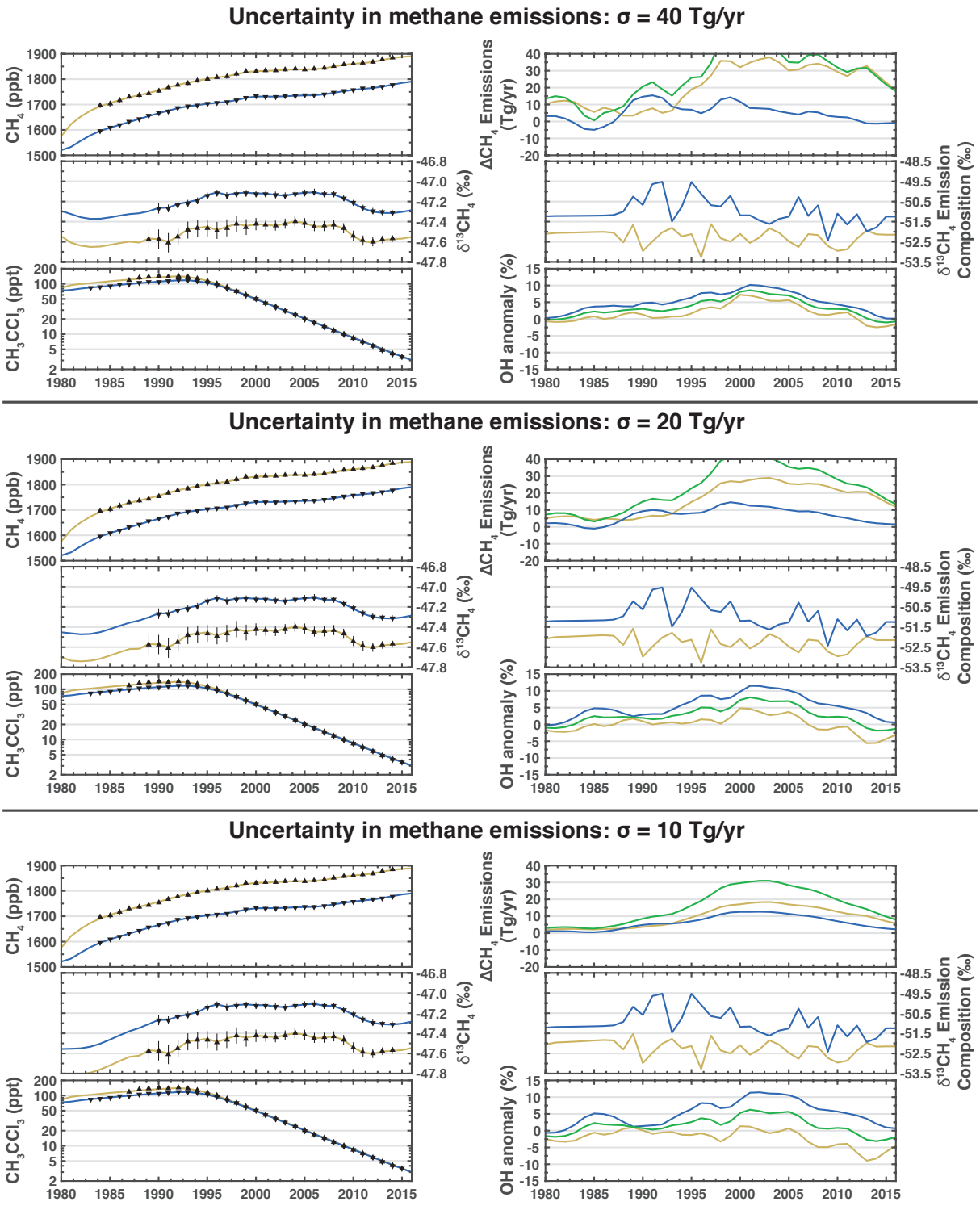

Figure 8: Varying the prior uncertainties in methane emissions. Each row is the same as main text Fig. 2 but using a linear Gaussian inversion with varying uncertainty in the methane emissions. Top row uses an uncertainty of 40 Tg/yr, middle row uses 20 Tg/yr, and bottom row uses 10 Tg/yr.

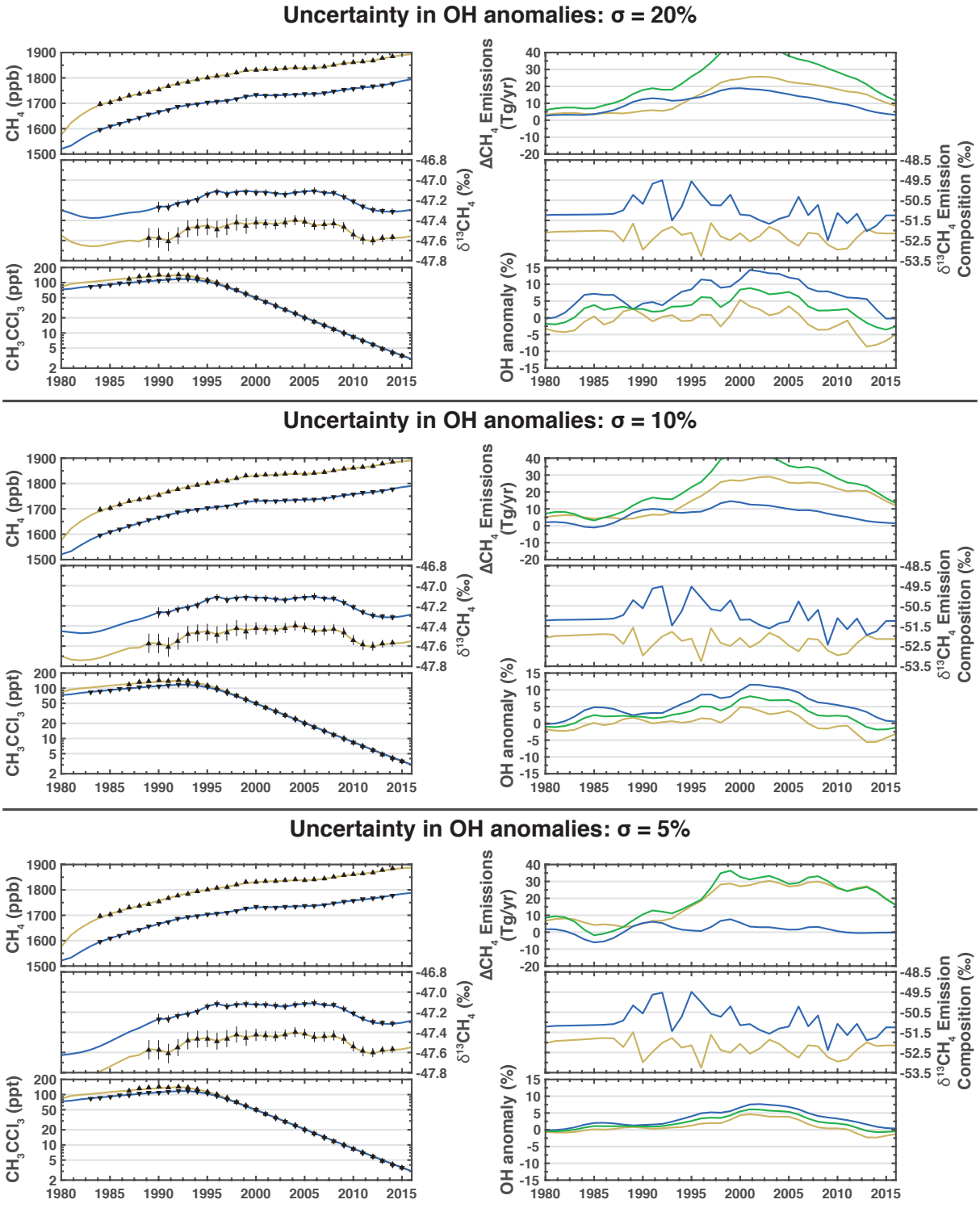

Figure 9: Varying the prior uncertainties in OH. Each row is the same as main text Fig. 2 but using a linear Gaussian inversion with varying uncertainty in the OH anomalies. Top row uses an uncertainty of 20%, middle row uses 10%, and bottom row uses 5%.

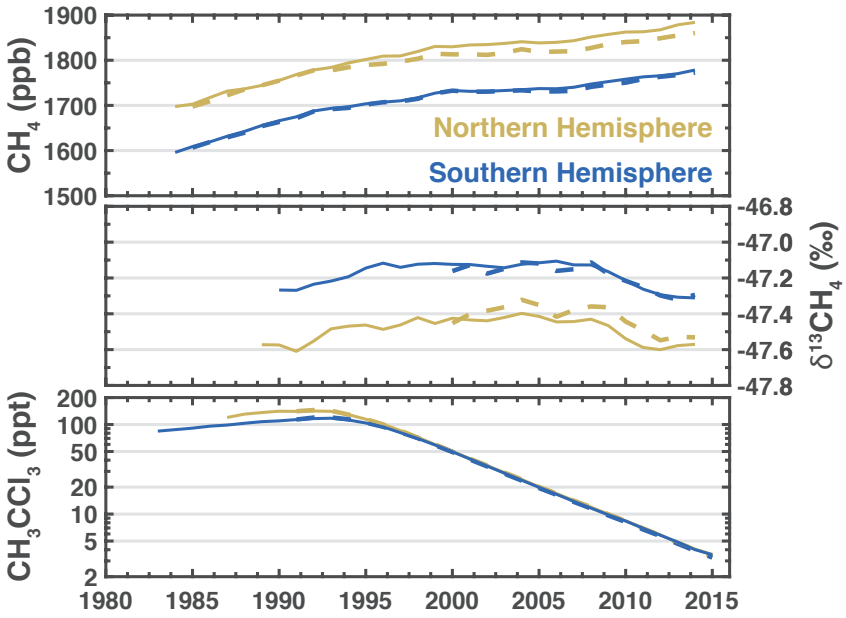

Figure 10: Comparison of the two hemispheric averaging schemes. Solid line is the bootstrapping scheme presented in Section 2 and dashed line is the alternate hemispheric average (E. Dlugokencky, NOAA/ESRL, personal communication; data included in tarball with code).

4.5 Varying the methyl chloroform reaction rate

We only consider the OH loss pathway for methyl chloroform (and methane). As such, the OH is representative of the entire loss term and induces an uncertainty in the appropriate reaction rate. The initial reaction rate was chosen to have a methyl chloroform lifetime of approximately 5.5 years[15], we use this as "Case A". We also test a case where we increased the methyl chloroform/OH reaction rate constant by 5%, resulting in a methyl chloroform lifetime of ∼5.3 years. The resulting methyl chloroform concentrations can be seen in the top row of Fig. S15 (simulated with the prior emissions).

Case A overestimates the methyl chloroform concentrations in the latter part of the record while Case B does a better job of simulating the methyl chloroform concentrations. However, there are also uncertainties in the methyl chloroform emissions in the latter part of the record. The prior emissions (dashed lines in the middle row of Fig. S15) shows that the prior assumes a simple exponential decay of the methyl chloroform emissions. A slightly faster rate of decay would also satisfy the methyl chloroform observations. This is exactly what happens in Case A. In Case A, the posterior emissions are reduced at a slightly faster rate than the prior emissions. The posterior simulations from both of these cases are able to reproduce the observations but they result in different emissions and OH anomalies (see Fig.16). We find that the change in the methane emissions and OH amonalies are about a factor of two less in Case B (reduced methyl chloroform lifetime).

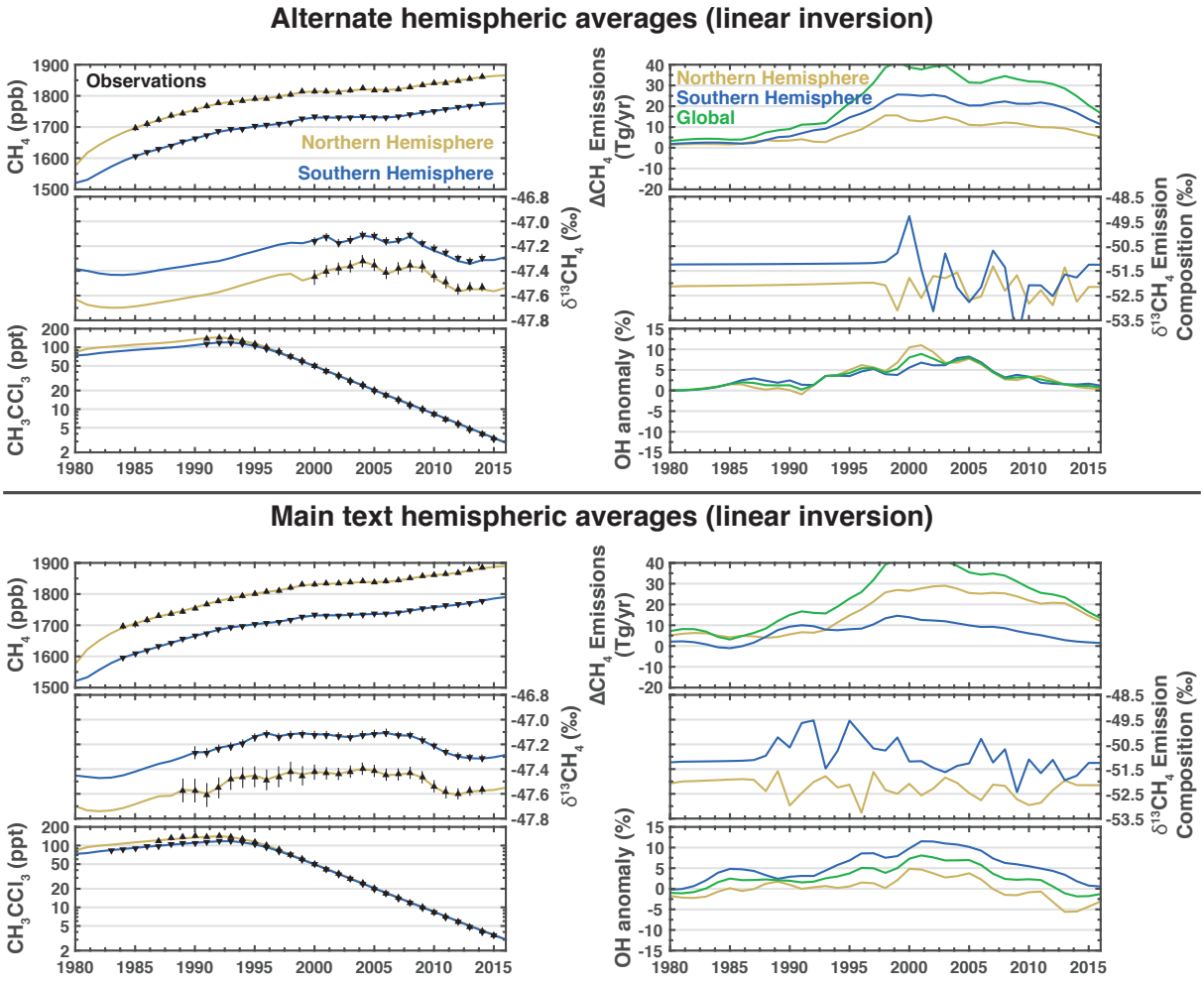

Figure 11: Linear Gaussian inversions with two different hemispheric averaging schemes. Top row uses the bootstrapping scheme presented in Section 2. Bottom row uses an alternate hemispheric averaging scheme (E. Dlugokencky, NOAA/ESRL, personal communication; data included in tarball with code).

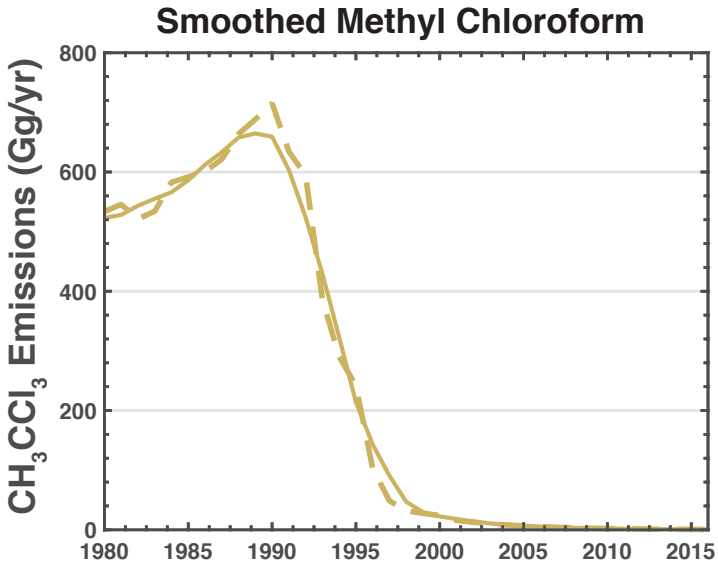

Figure 12: Smoothed methyl chloroform emissions. Dashed line is the emissions from Prinn *et al.*[14] and dashed line is smoothed using a 5-year filter.

5 Mechanistic explanation for the changes in OH

Changes in stratospheric ozone are a *potential* explanation for the decadal trends in OH. This is because changes in stratospheric ozone will affect $J\left(O^1D\right)$ and, in turn, tropospheric OH. Murray *et al.*[16] find that a 1% increase in stratospheric ozone leads to a 4.2% decrease in tropospheric OH (see Table 2 in Murray *et al.*[16]). Using this relationship and observations of stratospheric ozone from Mauna Loa (MLO), we can estimate the OH anomalies due to changes in stratospheric ozone.

Fig. 17 shows the OH anomalies inferred from stratospheric ozone at MLO, the OH anomalies from our "most likely solution", and the OH anomalies from McNorton *et al.*[17], Montzka *et al.*[18], and Rigby *et al.*[19]. While the magnitude of the OH anomalies inferred from stratospheric ozone at MLO is of the correct order the correlation is quite weak.

References

[1] Schaefer, H. *et al.* A 21st-century shift from fossil-fuel to biogenic methane emissions indicated by $^{13}CH_4$. *Science* **352**, 80–4 (2016).

[2] Rice, D. D. & Claypool, G. E. Generation, accumulation, and resource potential of biogenic gas. *Aapg Bulletin-American Association of Petroleum Geologists* **65**, 5–25 (1981).

[3] Martini, A. M., Budai, J. M., Walter, L. M. & Schoell, M. Microbial generation of economic accumulations of methane within a shallow organic-rich shale. *Nature* **383**, 155–158 (1996).

[4] Curtis, J. B. Fractured shale-gas systems. *Aapg Bulletin* **86**, 1921–1938 (2002).

[5] Stolper, D. A. *et al.* Gas formation. formation temperatures of thermogenic and biogenic methane. *Science* **344**, 1500–3 (2014).

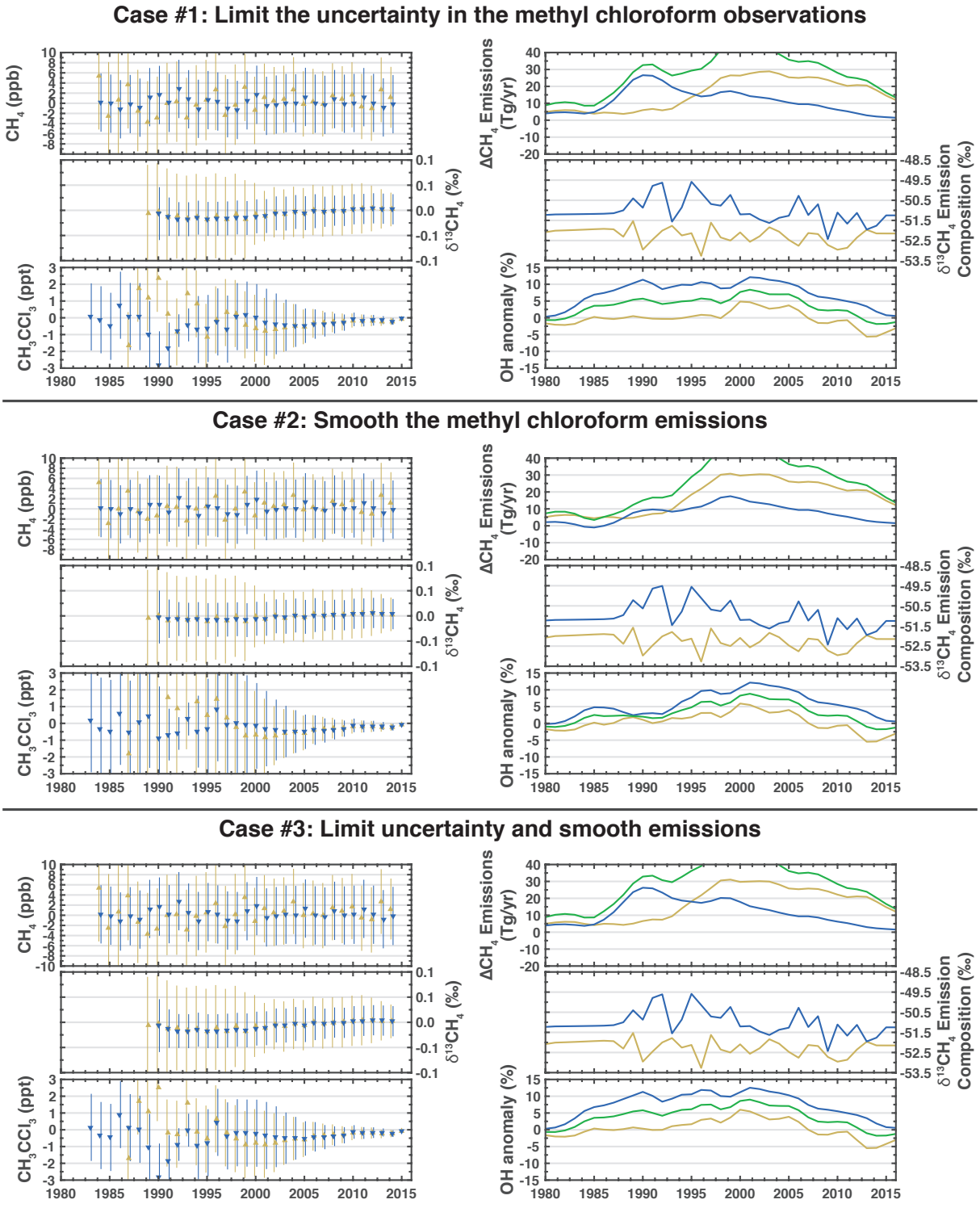

Figure 13: Results from the methyl chloroform sensitivity tests. Left column is the residuals and right column are the main drivers for the box model. Top panel is case 1. Middle panel is case 2. Bottom panel is case 3.

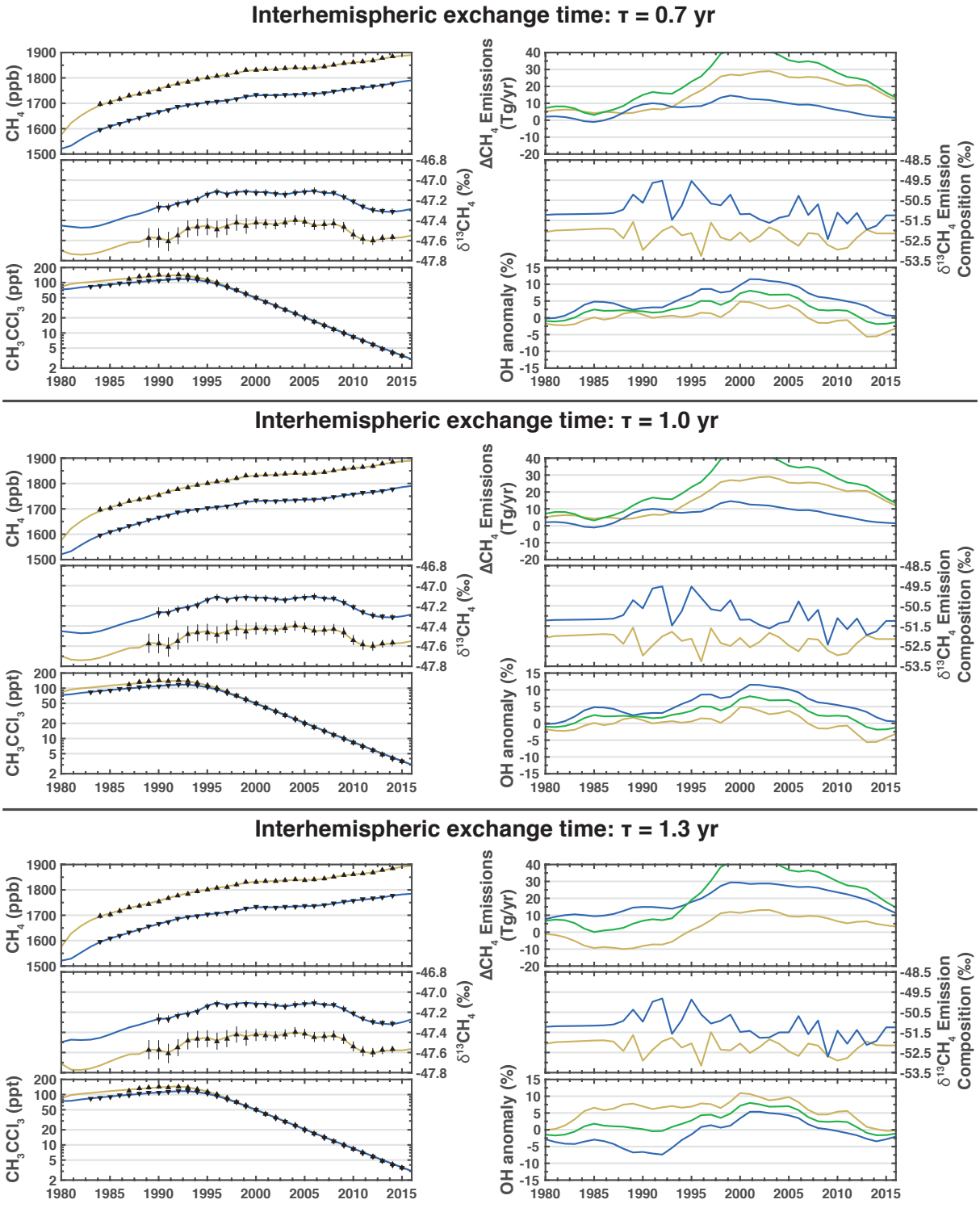

Figure 14: Varying the interhemispheric exchange time. Each row is the same as main text Fig. 2 but using a linear Gaussian inversion with varying interhemispheric exchange times (τ). Top row uses $\tau = 0.7$ yr, middle row uses $\tau = 1.0$ yr, and bottom row uses $\tau = 1.3$ yr.

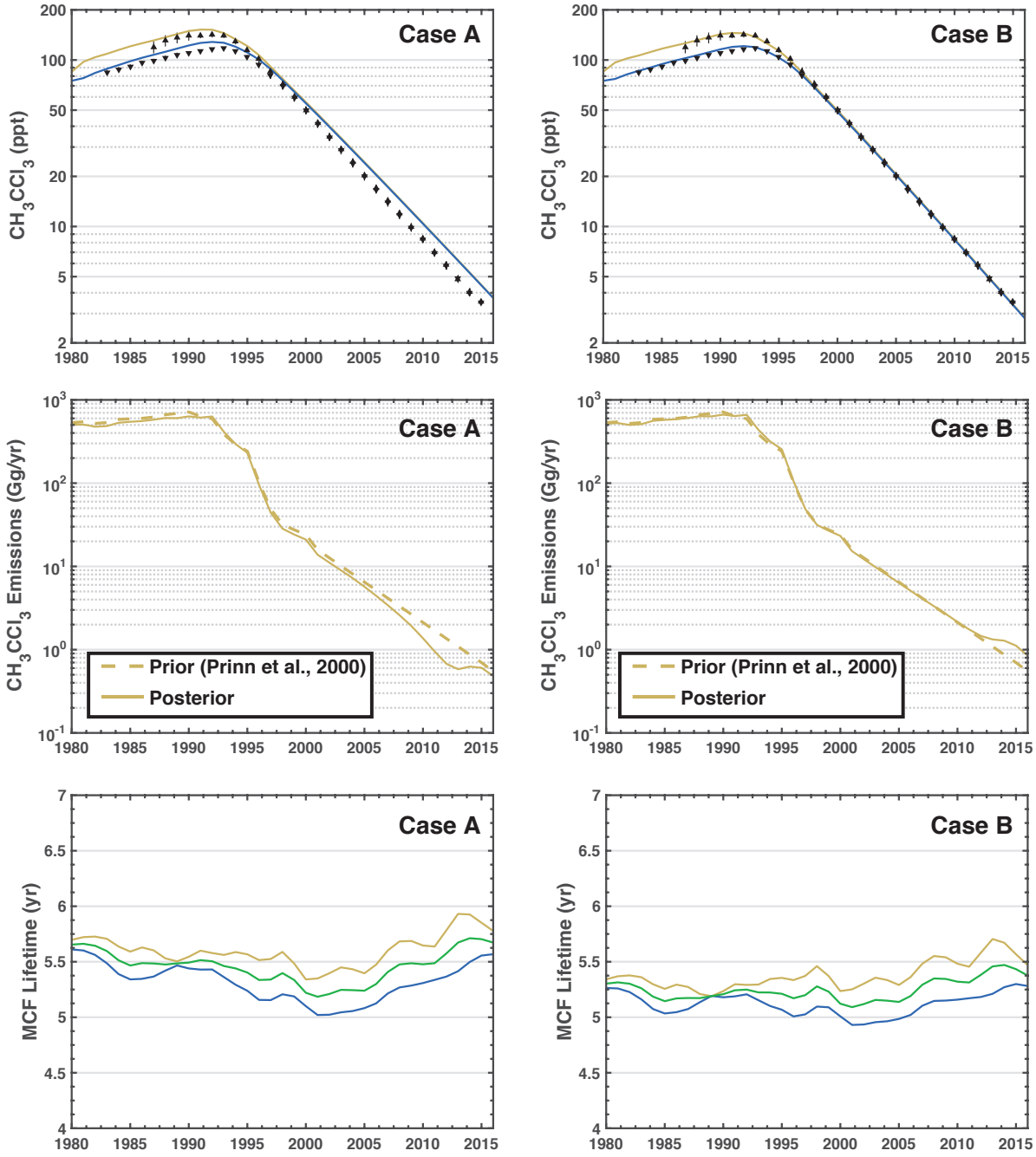

Figure 15: Varying the methyl chloroform reaction rate. Left column is with the Taldukar *et al.*[15] lifetime of 5.5 years and the right column is with a lifetime of ∼5.3 years. Top row shows the observed and simulated methyl chloroform observations. Middle row is the prior methyl chloroform emissions (dashed line) and posterior methyl chloroform emissions (solid line). Bottom panel is the methyl chloroform lifetimes in the posterior simulation.

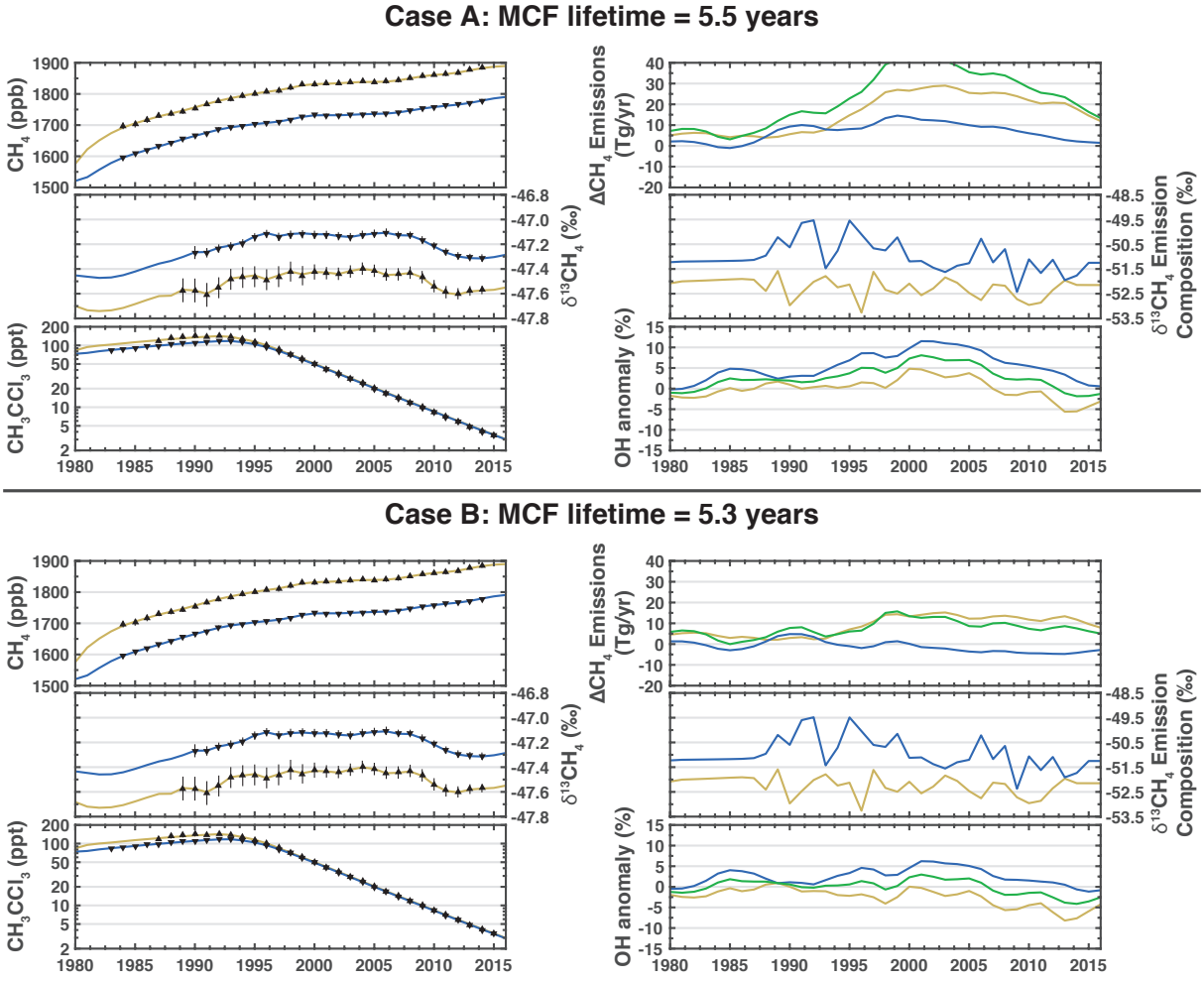

Figure 16: Varying the methyl chloroform reaction rate. Each row is the same as main text Fig. 2 but using a linear Gaussian inversion with varying methyl chloroform reaction rates. Top row results in a lifetime of 5.5 years[15] and the bottom row results in a lifetime of 5.3 years.

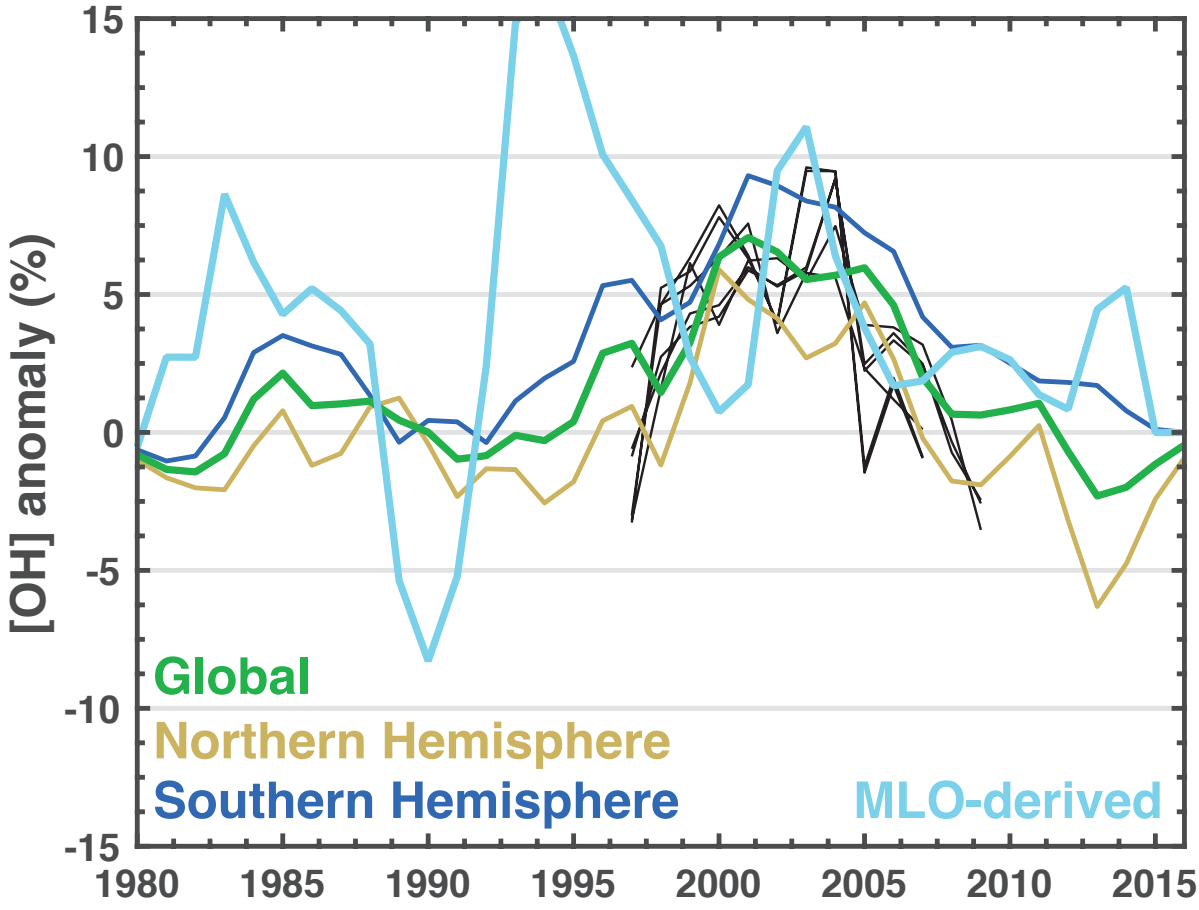

Figure 17: OH anomalies. Same as main text Fig. 3 but with the OH anomalies derived from stratospheric ozone observations at Mauna Loa (MLO-derived; cyan line).

[6] Wang, D. T. *et al.* Methane cycling. nonequilibrium clumped isotope signals in microbial methane. *Science* **348**, 428–31 (2015).

[7] Breas, O., Guillou, C., Reniero, F. & Wada, E. The global methane cycle: isotopes and mixing ratios, sources and sinks. *Isotopes Environ Health Stud* **37**, 257–379 (2001).

[8] Dlugokencky, E. J., Nisbet, E. G., Fisher, R. & Lowry, D. Global atmospheric methane: budget, changes and dangers. *Philos Trans A Math Phys Eng Sci* **369**, 2058–72 (2011).

[9] Schaefer, H. & Whiticar, M. J. Potential glacial-interglacial changes in stable carbon isotope ratios of methane sources and sink fractionation. *Global Biogeochemical Cycles* **22**, n/a–n/a (2008).

[10] Stolper, D. A. *et al.* Distinguishing and understanding thermogenic and biogenic sources of methane using multiply substituted isotopologues. *Geochimica et Cosmochimica Acta* **161**, 219–247 (2015).

[11] Schwietzke, S. *et al.* Upward revision of global fossil fuel methane emissions based on isotope database. *Nature* **538**, 88–91 (2016).

[12] Burkholder, J. B. *et al.* Chemical kinetics and photochemical data for use in atmospheric studies, evaluation no. 18. Tech. Rep., Jet Propulsion Laboratory (2015).

[13] Cantrell, C. A. *et al.* Carbon kinetic isotope effect in the oxidation of methane by the hydroxyl radical. *Journal of Geophysical Research-Atmospheres* **95**, 22455–22462 (1990).

[14] Prinn, R. G. *et al.* A history of chemically and radiatively important gases in air deduced from ALE/GAGE/AGAGE. *Journal of Geophysical Research: Atmospheres* **105**, 17751–17792 (2000).

[15] Talukdar, R. K. *et al.* Kinetics of the oh reaction with methyl chloroform and its atmospheric implications. *Science* **257**, 227–30 (1992).

[16] Murray, L. T., Logan, J. A. & Jacob, D. J. Interannual variability in tropical tropospheric ozone and OH: The role of lightning. *Journal of Geophysical Research: Atmospheres* **118**, 11,468–11,480 (2013).

[17] McNorton, J. *et al.* Role of OH variability in the stalling of the global atmospheric CH_4 growth rate from 1999 to 2006. *Atmospheric Chemistry and Physics* **16**, 7943–7956 (2016).

[18] Montzka, S. A. *et al.* Small interannual variability of global atmospheric hydroxyl. *Science* **331**, 67–9 (2011).

[19] Rigby, M. *et al.* Re-evaluation of the lifetimes of the major CFCs and CH_3CCl_3 using atmospheric trends. *Atmospheric Chemistry and Physics* **13**, 2691–2702 (2013).